IEEE Access
Multidisciplinary | Rapid Review | Open Access Journal

Date of publication xxxx 00, 0000, date of current version xxxx 00, 0000.

Digital Object Identifier 10.1109/ACCESS.2017.Doi Number

Anti-disturbance speed control of permanent magnet synchronous motor based on fractional order sliding mode load observer

En Lu[1, 2], Wei Li[2*], Song Jiang[2], Yufei Liu[2, 3]

[1] School of Agricultural Engineering, Jiangsu University, No. 301 Xuefu Road, Zhenjiang 212013, China
[2] School of Mechatronic Engineering, China University of Mining and Technology, No. 1 Daxue Road, Xuzhou 221116, China
[3] School of Artificial Intelligence, Anhui Polytechnic University, No. 8 Beijing Middle Road, Wuhu 241000, China

Corresponding author: Wei Li (e-mail: jsluen@163.com).

This work was supported by the National Natural Science Foundation of China (No. 52005220 and No. 51775543), China Postdoctoral Science Foundation Grant (2019M651962), and A Project Funded by the Priority Academic Program Development of Jiangsu Higher Education Institutions (No. PAPD-2018-87).

ABSTRACT Based on the fractional order sliding mode load observer, this paper presents an anti-disturbance speed control method of permanent magnet semi-direct drive transmission system for overhead manned equipment. According to the Lagrange equation, the dynamic model of semi-direct drive transmission system is established. Furthermore, the mathematical model of the permanent magnet synchronous motor (PMSM) is established based on the coordinate transformation theory. Subsequently, the fractional order sliding mode observer (FOSMO), which combines nonsingular terminal sliding mode control and fractional order theory is designed to observe the load disturbance changes in the permanent magnet semi-direct drive transmission system. Then, the concept of "active damping" is used to design the speed loop PI controller, and combined with the designed FOSMO to construct the composite speed controller. The designed composite speed controller is further improved by the anti-saturation design and parameter optimization. The results demonstrate that the designed FOSMO can precisely estimate the load disturbance on the PMSM output shaft. Additionally, the designed composite speed controller can realize stable speed control in the case of complex load disturbance, which meets the anti-disturbance speed control requirements of permanent magnet semi-direct drive transmission system, and the robustness of the control system is further improved by adding the anti-saturation link.

INDEX TERMS PMSM, anti-disturbance control, fractional order sliding mode, non-singular terminal sliding mode, load disturbance observer

I. INTRODUCTION

The overhead manned equipment is a continuous-action transport device pulled by the steel wire rope, and its schematic diagram is shown in Fig. 1. At present, the mining personnel of most coal enterprises go down to the downhole by means of the overhead manned equipment [1]. The traditional driving system of overhead manned equipment is the mode of "asynchronous motor + soft-start device + multistage reducer". As the core component, its reliability, stability and efficiency will directly affect the productivity and economic benefits of coal enterprises.

In recent years, the related technology of low-speed high-torque permanent magnet synchronous motors (PMSMs) is becoming more and more mature. Therefore, adopting the low-speed high-torque PMSM with better performance to replace the traditional asynchronous motor, and the multistage reducer can be replaced by single stage reducer. At this time, the PMSM, single stage reducer and other components constitute the permanent magnet semi-direct drive transmission system to shorten the transmission chain. This new driving system (as shown in Fig. 2) can not only reduce the vulnerable parts such as gears, but also improve the operational efficiency and reliability [2]. However, since the semi-direct drive transmission system reduces the transmission chain, the PMSM output shaft will bear more vibration and shock. It can cause speed control fluctuations, which in turn affect the stable operation and safety of overhead manned equipment.

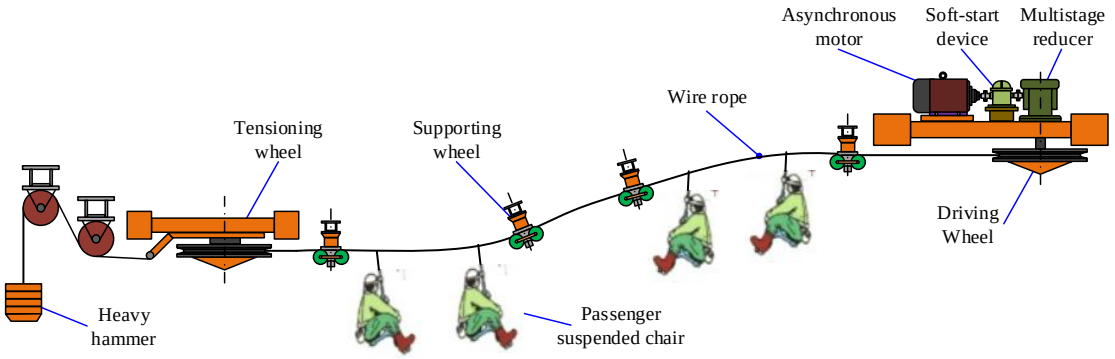

FIGURE 1. Schematic diagram of overhead manned equipment.

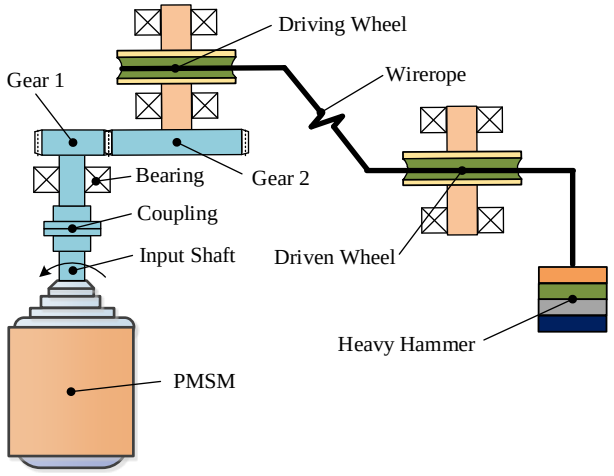

FIGURE 2. Schematic diagram of the permanent magnet semi-direct drive transmission system for overhead manned equipment.

With the development of PMSM technology and modern control theory, scholars at home and abroad have carried out a lot of research on speed control, and put forward many effective anti-disturbance speed control strategies. Petrovic et al. proposed a feedback law with adaptively estimating model parameters [3], which effectively suppresses the speed fluctuation in the PMSM system. Li et al. developed a modified internal model control (IMC) scheme based on the two-port IMC method, where a feedback control term is added to form a composite control structure [4]. It solves the problem of poor tracking and interference suppression performance of the standard IMC method when the control input is saturated. Yu et al. used dynamic surface control to reduce adaptive parameters, and combined with neural network to achieve anti-disturbance design in the case of parameter uncertainty and load disturbance of PMSM [5]. Sadala et al. presented a combination robust control algorithm of CNF control and super-twisting control (STC) methods [6], which shows better performance in tracking error, chattering suppression, robustness and so on. By introducing a fractional order terminal sliding mode surface, Wu et al. designed a novel fractional order terminal sliding mode controller for the speed loop to improve the PMSM speed tracking performance [7]. Lu et al. proposed a robust speed controller that combines the composite nonlinear feedback (CNF) and the integral sliding mode (ISM), which improves the transient responsive performance and robustness of the control system [8]. Xu et al. proposed a novel compensation scheme based on the integral sliding mode control (ISMC) theory for disturbance elimination. This proposed method incorporates the disturbance rejection term in the main control loop, which avoids the side effects of the traditional parallel external observer-based compensation method [9].

The compensation strategy based on disturbance identification is another effective anti-interference method. Tety et al. proposed a sixth-order discrete-time extended Kalman filter method for on-line estimation of speed, rotor position, load torque and stator resistance in the PMSM system [10]. Yu et al. used the neural networks to approximate the unknown and nonlinear functions of PMSM drive system [11]. Zhou et al. proposed an anti-disturbance robust control method based on the rapid nonlinear tracking differentiator (NTD) and disturbance observer (DOB) [12]. In the literature [13], a novel finite-time extended state observer (FTESO) combined with generalized super-twisting technique is constructed to estimate the unknown lumped disturbance and compensate the estimated value to the STSM speed controller. This method improves the anti-disturbance property and tracking performance of PMSM. Sun et al. designed a reduced-order observer based on additional disturbance state variables in discrete time to predict the future stator flux and observe the system disturbance caused by parameter mismatch [14]. However, like the full-order observer, this method still depends on the parameters of PMSM, and the observation accuracy cannot be guaranteed when the PMSM parameters are disturbed. The literatures [15, 16] designed the extended sliding mode observer (SMO) to estimate the load disturbances of PMSM. The SMO is a nonlinear method, which has the advantages of fast response speed, insensitivity to parameter changes and disturbances, strong robustness, and easy physical implementation. But the chattering of the sliding mode surface makes it difficult for the designed SMO to achieve the desired performance. Therefore, it is necessary to solve the chattering problem when using the SMO. Zhang et al. used the low-pass filter to suppress the effects of buffeting in the SMO [17]. Lu et al.

combined the advantages of both high-order sliding mode and non-singular terminal sliding mode, designing the second-order non-singular terminal sliding mode observer (SNTSMO) [18]. It realizes the fast convergence and no chattering observation of the load disturbance changes in the low-speed high-torque PMSM system. Ke et al. designed the SMO with multidimensional sliding mode surface to estimate the stator current and the lumped disturbance, and proposed the Hurwitz-based power reaching law (HPRL) to eliminate the uncertain disturbance calculation of classical power reaching law [19]. Compared with exponential reaching law, HPRL adopted in the SMO achieves high convergence rate and settles chattering.

The semi-direct drive transmission system reduces the transmission chain and vulnerable parts, but it also causes the PMSM output shaft to bear greater vibration impact. At the same time, the harsh underground environment of coal mine, vibration impact and high temperature will also cause the perturbation of system parameters, which further affect the stability of the control system. According to the above analysis, the SMO has the characteristics of strong robustness and insensitivity to parameter changes and disturbances. Therefore, it is more suitable for the permanent magnet semi-direct drive transmission system of the overhead manned equipment. Inspired by previous scholars' research, this paper presents an anti-disturbance speed control method for permanent magnet semi-direct drive transmission system of overhead manned equipment, and the main contributions are shown as follows: (a) According to the system structure and the coupling relationship between various components, and considering the nonlinear factors in the system, the nonlinear dynamic model of the semi-direct drive transmission system is established based on the Lagrange equation. The complex load characteristics on the output shaft of the PMSM can be obtained through this nonlinear dynamic model, which provides a basis for verifying the effectiveness of the designed composite speed controller. (b) On the basis of nonsingular terminal sliding mode control and fractional order control theory, this paper constructs the FOSMO to observe the load disturbance changes in the permanent magnet semi-direct drive transmission system, and the observed value is used as the compensation control input. Moreover, the fast power reaching law with second-order sliding mode characteristics is adopted to reduce the chattering of the sliding mode surface to improve the accuracy of load disturbance observation. (c) Aiming at the problem of difficult selection of controller parameters, the concept of "active damping" is used to design the speed loop PI controller, and the goal of simpler parameter tuning is achieved. At the same time, based on the ITAE index, the hybrid PSO algorithm is used to optimize the parameters of the FOSMO. Furthermore, in order to ensure that the permanent magnet semi-direct drive transmission system has better anti-disturbance performance, the anti-saturation improvement of the composite speed controller is also carried out in this paper. Finally, the effectiveness of the proposed method is verified based on the load characteristics of the permanent magnet semi-direct drive transmission system of the overhead manned equipment.

This paper intends to realize the anti-disturbance speed control of the permanent magnet semi-direct drive transmission system based on FOSMO. In Section 2, the mathematical models of PMSM and semi-direct drive transmission system are presented. Section 3 presents the design of FOSMO, which is based on the fractional order theory and the non-singular terminal sliding mode method. According to the designed PI controller and FOSMO in Section 4, the anti-disturbance composite speed controller is established. Section 5 presents the results and analysis of the designed FOSMO and anti-disturbance composite speed controller for the permanent magnet semi-direct drive transmission system. The brief conclusions are drawn in Section 6.

II. MATHEMATICAL MODELING

A. MATHEMATICAL MODELING OF SEMI-DRIVE TRANSMISSION SYSTEM

According to the system structure and the coupling relationship between various components, the permanent magnet semi-direct drive transmission system of the overhead manned equipment can be divided into PMSM and gear 1 unit, gear 1 and gear 2 meshing unit, gear 2 and load unit. Its dynamic model can be simplified into a massless spring system with certain stiffness and damping through the lumped parameter method. Among them, the motor rotor includes 1 rotation degree of freedom, gear 1 and gear 2 include 4 translational and 2 rotational degrees of freedom, and the load includes 1 rotation degree of freedom. According to the Lagrange equation, the following dynamic model can be established [20]:

$$\begin{cases} J_m\ddot{\theta}_m + c_a\left(\dot{\theta}_m - \dot{\theta}_1\right) + k_a\left(\theta_m - \theta_1\right) = T_e \\ m_1\ddot{x}_1 + c_{x1}\dot{x}_1 + k_{x1}x_1 = F_{12}\cos\delta_{12} \\ m_1\ddot{y}_1 + c_{y1}\dot{y}_1 + k_{y1}y_1 = -F_{12}\sin\delta_{12} \\ J_1\ddot{\theta}_1 - c_a\left(\dot{\theta}_m - \dot{\theta}_1\right) - k_a\left(\theta_m - \theta_1\right) = -F_{12}R_1 \\ m_2\ddot{x}_2 + c_{x2}\dot{x}_2 + k_{x2}x_2 = -F_{12}\cos\delta_{12} \\ m_2\ddot{y}_2 + c_{y2}\dot{y}_2 + k_{y2}y_2 = F_{12}\sin\delta_{12} \\ J_2\ddot{\theta}_2 + c_b\left(\dot{\theta}_2 - \dot{\theta}_L\right) + k_b\left(\theta_2 - \theta_L\right) = F_{12}R_2 \\ J_L\ddot{\theta}_L - c_b\left(\dot{\theta}_2 - \dot{\theta}_L\right) - k_b\left(\theta_2 - \theta_L\right) = -T_L \end{cases} \tag{1}$$

where J_m, J_1, J_2 and J_L are the rotational inertia of PMSM, gear 1, gear 2 and load driving wheel, respectively; m_1 and m_2 are the masses of gear 1 and gear 2 respectively; θ_m, θ_1, θ_2 and θ_L is the rotation angle of PMSM, gear 1, gear 2 and load driving wheel respectively; x_1, y_1, x_2 and y_2 are the displacement of gear 1 and gear 2 on the x-axis and y-axis respectively; c_a and c_b torsional damping of the motor

output shaft and the semi-direct drive transmission system output shaft; c_{x1}, c_{y1}, c_{x2}、c_{y2} are the support damping of gear 1 and gear 2 on the *x*-axis and *y*-axis respectively; k_a and k_b are the torsional stiffness of the motor output shaft and the semi-direct drive transmission system output shaft respectively; k_{x1}, k_{y1}, k_{x2} and k_{y2} are the support stiffness of gear 1 and gear 2 on the *x*-axis and *y*-axis respectively; R_1 and R_2 are the base circle radius of gear 1 and gear 2 respectively; T_e and T_L are the electromagnetic torque of PMSM and the load torque of load driving wheel respectively; F_{12} is the meshing force of gear pair (gear 1 and gear 2); δ_{12} is the dynamic transmission error of the gear pair (gear 1 and gear 2).

Dynamic transmission error δ_{12} of the gear pair in (1) can be expressed as follows.

$$\begin{aligned}\delta_{12} = &-\cos\alpha_{12}x_1 + \sin\alpha_{12}y_1 + \cos\alpha_{12}x_2 \\ &-\sin\alpha_{12}y_2 + R_1\theta_1 - R_2\theta_2 - e_{12}\end{aligned} \tag{2}$$

where α_{12} is the gear pressure angle, e_{12} is the static transmission error.

Due to the existence of manufacturing and installation errors, the semi-direct drive transmission system has impact phenomenon during gear meshing, which will affect the stability of the transmission system. The backlash function can be expressed as follows [21].

$$f(\delta_{12}) = \begin{cases} \delta_{12} - b & \delta_{12} > b \\ 0 & -b \le \delta_{12} \le b \\ \delta_{12} + b & \delta_{12} < -b \end{cases} \tag{3}$$

where b is the backlash.

The meshing force F_{12} of gear pair is composed of the elastic force caused by gear meshing stiffness and the viscous force caused by meshing damping, expressed as follows.

$$F_{12} = k_{12} f(\delta_{12}) + c_{12}\dot{\delta}_{12} \tag{4}$$

B. MATHEMATICAL MODELING OF PMSM

PMSM is a typical nonlinear strongly coupled system, which contains multiple variable parameters in the mathematical model in the natural coordinate system. The Clark transformation and Park transformation are applied to simplify its mathematical model. Finally, the stator voltage equation of PMSM in the *d*-*q* synchronous reference frame can be established as follows [8].

$$\begin{cases} u_d = R_s i_d + L_d \dot{i}_d - \omega_e L_q i_q \\ u_q = R_s i_q + L_q \dot{i}_q + \omega_e L_d i_d + \omega_e \psi_f \end{cases} \tag{5}$$

where u_d and u_q are the stator voltage components on the *d*-*q* axis, i_d and i_q are the stator current components on the *d*-*q* axis, L_d and L_q are the inductances on the *d*-*q* axis, R_s is the stator resistance, ω_e is the electric angular speed, ψ_f is the flux linkage, respectively.

The electromagnetic torque of PMSM is shown as follows.

$$T_e = 1.5 p_n i_q [i_d (L_d - L_q) + \psi_f] \tag{6}$$

where p_n is the number of pole pairs. For the surface-mounted PMSM, if the control method of i_d=0 is used, the (6) can be simplified as follows.

$$T_e = 1.5 p_n \psi_f i_q \tag{7}$$

The motion equation of PMSM is shown as follows [4].

$$T_e - T_{Lm} = B_m \omega_m + J_m \dot{\omega}_m \tag{8}$$

where T_{Lm} is the load torque of PMSM, B_m is the viscous friction coefficient, ω_m is the mechanical angular speed, J_m is the rotational inertia, respectively.

III. MATHEMATICAL MODELING DESIGN OF LOAD DISTURBANCE OBSERVER

There are various internal and external disturbances in the actual permanent magnet semi-direct drive transmission system of the overhead manned equipment, such as load torque, damping torque, parameter perturbation, and so on. These disturbances more or less affect the control performance of the permanent magnet semi-direct drive transmission system, and then affect the stable and safe operation of the overhead manned equipment. Generally, the load torque is much larger than the sum of other disturbances and plays a leading role in the disturbances. If the friction coefficient B_m is ignored, the speed change of PMSM can be expressed as follows [18].

$$\omega_m = \frac{1}{J_m}\int_{t_0}^{t}(T_e - T_{Lm})dt = \frac{1}{J_m}\int_{t_0}^{t}\Delta T dt \tag{9}$$

Equation (9) shows that the fluctuation changes of ΔT can cause the fluctuation of speed. From the perspective of control, the stable speed control of permanent magnet semi-direct drive transmission system needs to realize the electromagnetic torque to track the change of load torque well. Therefore, it is necessary to estimate the load disturbance and compensate it to the speed control system.

A. DESIGN OF FOSMO

Combined with the (7) and (8), and taking the load torque as the extended state variable, the extended state equation of PMSM can be established as follows [15].

$$\begin{cases} \dot{\omega}_m = \frac{1}{J_m}\left(1.5 p_n \psi_f i_q - T_{Lm} - B_m \omega_m\right) \\ \dot{T}_{Lm} = 0 \end{cases} \tag{10}$$

Based on the sliding mode control theory which is insensitive to the disturbances and parameter perturbation and has fast response speed, the FOSMO is designed to observe the load torque of PMSM, and shown as follows [17].

$$\begin{cases} \dot{\hat{\omega}}_m = \frac{1}{J_m}\left(1.5 p_n \psi_f i_q - \hat{T}_{Lm} - B_m \hat{\omega}_m\right) + u_{smo} \\ \dot{\hat{T}}_{Lm} = g u_{smo} \end{cases} \tag{11}$$

where u_{smo} is the switching function of sliding mode control, g is the sliding mode coefficient, $\hat{\omega}_m$ is the observed value of angular speed of PMSM, and $\hat{T}_{Lm}$ is the observed value of load torque of PMSM.

The observation errors of the FOSMO can be obtained by subtracting the (10) from the (11), and shown as follows.

$$\begin{cases} \dot{\tilde{\omega}}_m = \dfrac{1}{J_m}\left(-\tilde{T}_{Lm} - B_m\tilde{\omega}_m\right) + u_{smo} \\ \dot{\tilde{T}}_{Lm} = g u_{smo} \end{cases} \tag{12}$$

where $\tilde{\omega}_m = \hat{\omega}_m - \omega_m$ and $\tilde{T}_{Lm} = \hat{T}_{Lm} - T_{Lm}$ are the observation errors of the angular speed and load torque, respectively.

The research in recent years has shown that most real complex systems have fractional order properties, so it is more reasonable and accurate to describe the system in the form of fractional calculus. Besides, compared with integer order control, fractional order control has stronger anti-disturbance performance, dynamic and static response ability. The fractional calculus combines differential and integral operations, which can be expressed by the following unified fractional operators [22]:

$${}_{t_0}D_t^{\mu} = \begin{cases} \dfrac{d^{\mu}}{dt^{\mu}}, & \mathrm{Re}(\mu) > 0 \\ 1, & \mathrm{Re}(\mu) = 0 \\ \int_{t_0}^{t} (d\tau)^{-\mu}, & \mathrm{Re}(\mu) < 0 \end{cases} \tag{13}$$

where t_0 and t are the lower and upper limits of fractional calculus respectively; μ is the order of fractional calculus, which can be any real number or complex number; Re (•) stands for the real ministry. In this paper, the order μ is a real number. From the (13), it can be seen that when μ>0, fractional calculus operator represents differential, when μ<0, fractional calculus operator represents integral.

Due to the influence of the switching function sgn in SMO, the chattering will occur in the sliding mode plane switching process, and the traditional SMO is closer to the equilibrium point, the slower the system state converging. Therefore, the sliding mode surface is the main determinant of the dynamic performance of SMO. The nonsingular terminal sliding mode has clear physical significance, which can ensure that the system is able to reach the sliding mode surface and reach the system zero point in a limited time. Compared with the linear sliding mode, the nonsingular terminal sliding mode has the advantages of smaller sliding mode switching gain, faster convergence speed, higher system stability accuracy and stronger robustness. On the basis of nonsingular terminal sliding mode control [15] and fractional order theory [22], according to the speed estimation error $\tilde{\omega}_m$, the sliding mode surface is constructed as follows.

$$s = \tilde{\omega}_m + \frac{1}{\beta}({}_0D_t^{\mu}\tilde{\omega}_m)^{p/q} \tag{14}$$

where β>0, 0<μ<1, p and q (p>q) are positive odd number. The derivative of the (14) with respect to time is shown as follows.

$$\dot{s} = \dot{\tilde{\omega}}_m + \frac{1}{\beta}\frac{p}{q}({}_0D_t^{\mu}\tilde{\omega}_m)^{p/q-1}({}_0D_t^{1+\mu}\tilde{\omega}_m) \tag{15}$$

In order to reduce the chattering of the sliding mode surface, a fast power reaching law with second-order sliding mode characteristics is selected to ensure that the better dynamic characteristics in reaching stage [23]. The fast power reaching law is shown as follows [24].

$$slaw = -k_{f1}|s|^{\alpha}\,\mathrm{sgn}(s) - k_{f2}s = \dot{s} \quad k_{f1}>0,\ k_{f2}>0 \tag{16}$$

where k_{f1}>0, k_{f2}>0, $\alpha \in (0, 1)$.

According to the (14) and (16), the sliding mode control law of FOSMO can be designed as follows [25].

$$u_{smo} = u_{eq} + u_n \tag{17}$$

where $u_n = -{}_0D_t^{-\mu}\left(\dfrac{\beta q}{p}({}_0D_t^{\mu}\tilde{\omega}_m)^{2-p/q} + k_{f1}|s|^{\alpha}\,\mathrm{sgn}(s) + k_{f2}s\right)$,

$u_{eq} = \dfrac{B_m}{J_m}\tilde{\omega}_m$.

B. STABILITY ANALYSIS OF FOSMO

In order to analyze stability of the designed FOSMO, the following Lyapunov function is selected:

$$V = \frac{1}{2}s^2 \tag{18}$$

The derivative of the (18) with respect to time is shown as follows.

$$\begin{aligned} \dot{V} &= s\cdot\dot{s} \\ &= s\cdot\left(\dot{\tilde{\omega}}_m + \frac{1}{\beta}\frac{p}{q}({}_0D_t^{\mu}\tilde{\omega}_m)^{p/q-1}({}_0D_t^{1+\mu}\tilde{\omega}_m)\right) \\ &= s\cdot\frac{p}{\beta q}({}_0D_t^{\mu}\tilde{\omega}_m)^{p/q-1}\left({}_0D_t^{1+\mu}\tilde{\omega}_m + \frac{\beta q}{p}({}_0D_t^{\mu}\tilde{\omega}_m)^{2-p/q}\right) \end{aligned} \tag{19}$$

Substituting the (17) into the (12), the (12) can be rewritten as follows.

$$\dot{\tilde{\omega}}_m = -\frac{1}{J_m}\tilde{T}_{Lm} + u_n \tag{20}$$

Therefore, the fractional order of the (20) can be expressed as follows.

$${}_0D_t^{1+\mu}\tilde{\omega}_m = -\frac{1}{J_m}{}_0D_t^{\mu}\tilde{T}_{Lm} + {}_0D_t^{\mu}u_n \tag{21}$$

Substituting the (21) and (17) into the (19), the (19) can be rewritten as follows.

$$\begin{aligned} \dot{V} &= s\cdot\frac{p}{\beta q}({}_0D_t^{\mu}\tilde{\omega}_m)^{p/q-1}\left(-\frac{1}{J_m}{}_0D_t^{\mu}\tilde{T}_{Lm} + {}_0D_t^{\mu}u_n + \frac{\beta q}{p}({}_0D_t^{\mu}\tilde{\omega}_m)^{2-p/q}\right) \\ &= s\cdot\frac{p}{\beta q}({}_0D_t^{\mu}\tilde{\omega}_m)^{p/q-1}\left(-\frac{1}{J_m}{}_0D_t^{\mu}\tilde{T}_{Lm} - k_{f1}|s|^{\alpha}\,\mathrm{sgn}(s) - k_{f2}s\right) \\ &= -\frac{p}{\beta q}({}_0D_t^{\mu}\tilde{\omega}_m)^{p/q-1}\left(\frac{1}{J_m}{}_0D_t^{\mu}\tilde{T}_{Lm}\cdot s + k_{f1}|s|^{\alpha}\,\mathrm{sgn}(s)\cdot s + k_{f2}s\cdot s\right) \\ &= -\frac{p}{\beta q}({}_0D_t^{\mu}\tilde{\omega}_m)^{p/q-1}\left(\frac{1}{J_m}{}_0D_t^{\mu}\tilde{T}_{Lm}\cdot s + k_{f1}|s|^{1+\alpha} + k_{f2}s^2\right) \end{aligned} \tag{22}$$

Since p and q are odd numbers, and p>q>0, only when ${}_0D_t^{\mu}\tilde{\omega}_m = 0$, $({}_0D_t^{\mu}\tilde{\omega}_m)^{p/q-1} = 0$, otherwise $({}_0D_t^{\mu}\tilde{\omega}_m)^{p/q-1} > 0$. Equation (22) can be expressed in the following two forms [18].

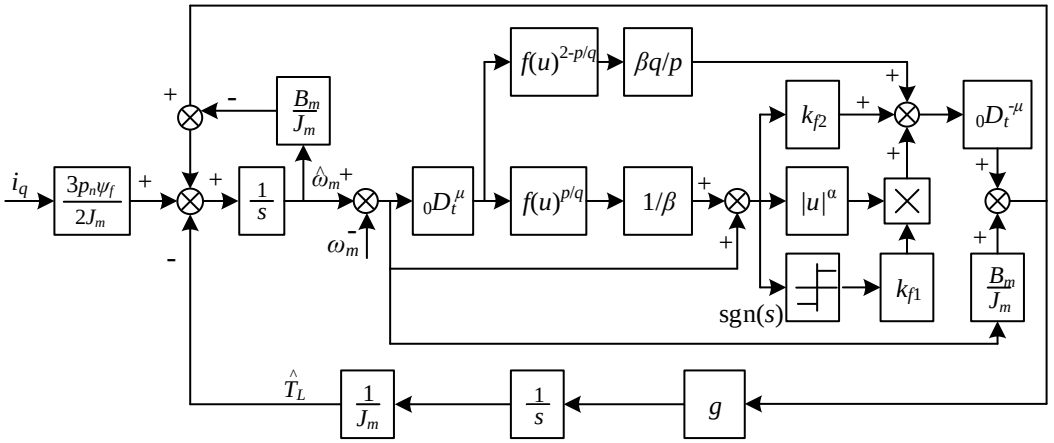

FIGURE 3. Schematic diagram of the designed FOSMO.

$$\dot{V} \le -\frac{p}{\beta q}({}_0D_t^{\mu}\tilde{\omega}_m)^{p/q-1}\left(-\left|\frac{1}{J_m}{}_0D_t^{\mu}\tilde{T}_{Lm}\right|\cdot|s|+k_{f1}|s|^{1+\alpha}+k_{f2}|s|^2\right) \tag{23}$$
$$=-\frac{p}{\beta q}({}_0D_t^{\mu}\tilde{\omega}_m)^{p/q-1}\left(k_{f1}|s|^{1+\alpha}+|s|\cdot\left(k_{f2}|s|-\left|\frac{1}{J_m}{}_0D_t^{\mu}\tilde{T}_{Lm}\right|\right)\right)$$

$$\dot{V} \le -\frac{p}{\beta q}({}_0D_t^{\mu}\tilde{\omega}_m)^{p/q-1}\left(-\left|\frac{1}{J_m}{}_0D_t^{\mu}\tilde{T}_{Lm}\right|\cdot|s|+k_{f1}|s|^{1+\alpha}+k_{f2}|s|^2\right) \tag{24}$$
$$=-\frac{p}{\beta q}({}_0D_t^{\mu}\tilde{\omega}_m)^{p/q-1}\left(|s|\cdot\left(k_{f1}|s|^{\alpha}-\left|\frac{1}{J_m}{}_0D_t^{\mu}\tilde{T}_{Lm}\right|\right)+k_{f2}|s|^2\right)$$

It is assumed that the $\left|\frac{1}{J_m}{}_0D_t^{\mu}\tilde{T}_{Lm}\right| \le M$, and $M \ge 0$. For the (23), when $k_{f1}|s|-M \ge 0$, then $\dot{V} \le 0$. According to the comparative lemma [26], the designed FOSMO can reach and maintain the non-singular terminal sliding mode state in a limited time (s=0), so that the system can achieve the $\tilde{\omega}_m = 0$ in a limited time. Therefore,

$$|s| \le \frac{M}{k_{f2}} \tag{25}$$

According to the (24), through the same analysis method, it can be obtained:

$$|s| \le \left(\frac{M}{k_{f1}}\right)^{\frac{1}{\alpha}} \tag{26}$$

According to the (25) and (26), the convergence region of sliding mode surface s in a limited time can be expressed as follows [23].

$$|s| \le \min\left(\left(\frac{M}{k_{f1}}\right)^{\frac{1}{\alpha}}, \frac{M}{k_{f2}}\right) \tag{27}$$

Combined with the (16), the convergence region of the first derivative of the sliding mode surface s in a limited time can be expressed as follows [23].

$$|\dot{s}| \le k_{f1}|s|^{\alpha}+k_{f2}|s|$$
$$\le k_{f1}\cdot\min\left(\left(\frac{M}{k_{f1}}\right)^{\frac{1}{\alpha}}, \frac{M}{k_{f2}}\right)^{\alpha}+k_{f2}\cdot\min\left(\left(\frac{M}{k_{f1}}\right)^{\frac{1}{\alpha}}, \frac{M}{k_{f2}}\right) \tag{28}$$
$$=\min\left(M, k_{f1}\left(\frac{M}{k_{f2}}\right)^{\alpha}\right)+\min\left(k_{f2}\left(\frac{M}{k_{f1}}\right)^{\frac{1}{\alpha}}, M\right)$$

It is assumed that the convergence time of the sliding mode surface s from the initial value to 0 is t_r. When $t>t_r$, ω_m will enter the terminal sliding mode motion state and converge to zero after time t_s. The total convergence time of the designed FOSMO can be expressed as follows [25].

$$t = t_r + t_s = t_r + \beta\frac{p}{p-q}\max\left(\left|{}_0D_t^{\mu}\tilde{\omega}_m(t_r)^{1-p/q}\right|\right) \tag{29}$$

According to the (29), the convergence speed of the designed FOSMO can be adjusted by selecting the parameters β, p and q on the sliding mode surface s.

The schematic diagram of the designed FOSMO is shown in Fig. 3.

C. PARAMETER OPTIMIZATION OF FOSMO

Although the selection range of parameters in the FOSMO can be determined through stability analysis, the selected parameters may not guarantee the optimal performance of the FOSMO. Therefore, this paper uses the PSO algorithm to optimize the parameters of FOSMO. The ITAE index is selected as the fitness function to ensure that the FOSMO has good performance [27], and shown as follows.

$$F_{pso} = \int_{t_0}^{t} t\left|\tilde{T}_{Lm}\right| dt \tag{30}$$

PSO algorithm is a relatively new branch of swarm intelligence. It was proposed by Kennedy and Eberhart in 1995 [28]. It is a method to find the optimal solution by simulating the bird colony to find habitat. Its core idea is to use the information sharing mechanism to learn from the experience of each particle to realize the development of the population. Each member of the population in the PSO

algorithm is called a particle, and each particle represents a potential feasible solution. The flight direction of each particle is adjusted by the fitness function value and velocity to ensure that the particles can fly to the globally optimal position.

In the *D*-dimensional search space, the position and velocity of the i_{th} particle are expressed as $X_i = [x_{i1}, x_{i2}, \ldots, x_{iD}]$, $V_i=[v_{i1}, v_{i2}, \ldots, v_{iD}]$, respectively. In the process of evolutionary search, the position of i_{th} particle is adjusted according to the current velocity, personal history best position ($pbest_i$) and global best position ($gbest$). Among them, $pbest_i = [\, pbest_i^1, pbest_i^2, \ldots, pbest_i^d]$, $gbest = [\, gbest^1, gbest^2, \ldots, gbest^d]$. The velocity and position of the i_{th} particle in dimension D can be updated through the (31) and (32) [29], and the principle is shown in Fig. 4.

$$v_i^d(t+1) = w \cdot v_i^d(t) + c_1 \cdot rand_1^d \cdot (pbest_i^d(t) - x_i^d(t)) + c_2 \cdot rand_2^d \cdot (gbest^d(t) - x_i^d(t)) \quad (31)$$

$$x_i^d(t+1) = x_i^d(t) + v_i^d(t+1) \quad (32)$$

where w is the inertia factor, c_1 and c_2 are the acceleration factors, and $rand_1^d$ and $rand_2^d$ are uniformly distributed random numbers within the range of [0, 1].

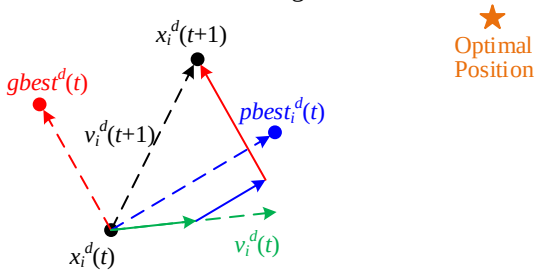

FIGURE 4. Iteration scheme of the particles in the PSO algorithm.

The above basic PSO algorithm has the advantages of easy physical implementation, fast convergence speed and few parameters. But, due to the lack of individual diversity and high-quality solutions, the basic PSO algorithm may converge prematurely and fall into local optimization in the face of complex optimization problems [30]. The crossover operation is one of the three genetic operations in the Genetic algorithm, and it is the key to determine the convergence performance of the algorithm [31]. In this paper, the crossover operation is mixed into the basic PSO algorithm, and it is added after the speed and position update respectively, as shown in (33) and (34). The newly added crossover operation in the hybrid PSO algorithm enables the offspring particles to inherit the advantages of the parent particles, and theoretically strengthens the search ability of the region between particles. Therefore, the particles in the local optimal region can get rid of the local optimal, so as to improve the search results.

$$\begin{cases} v_i^d(t) = rand_3^d \cdot v_i^d(t+1) + (1 - rand_3^d) \cdot v_i^d(t) \\ v_i^d(t+1) = rand_4^d \cdot v_i^d(t) + (1 - rand_4^d) \cdot v_i^d(t+1) \end{cases} \quad (33)$$

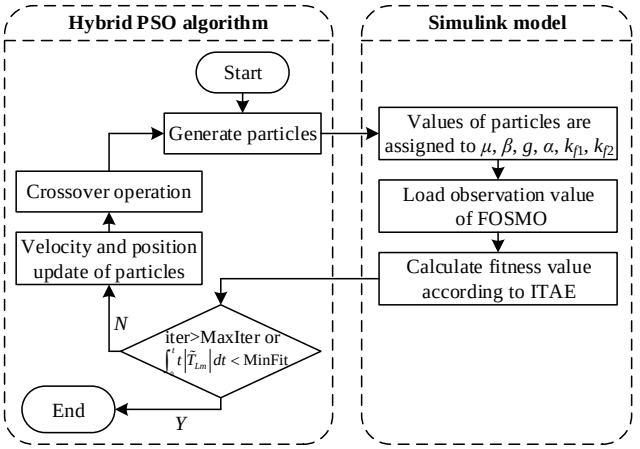

FIGURE 5. Schematic diagram of parameter optimization of FOSMO based on the hybrid PSO algorithm.

$$\begin{cases} x_i^d(t) = rand_5^d \cdot x_i^d(t+1) + (1 - rand_5^d) \cdot x_i^d(t) \\ x_i^d(t+1) = rand_6^d \cdot x_i^d(t) + (1 - rand_6^d) \cdot x_i^d(t+1) \end{cases} \quad (34)$$

Based on the above hybrid PSO algorithm, the parameters of the designed FOSMO are optimized, and the schematic diagram is shown in Fig. 5.

IV. DESIGN OF SPEED CONTROLLER

A. DESIGN OF PI SPEED CONTROLLER

According to the concept of "active damping" proposed in document [32], the parameters of the speed loop PI controller are designed, and defined as follows.

$$i_q^* = i_q' - B_a \omega_m \quad (35)$$

It is assumed that the PMSM starts under no-load condition (T_{Lm}=0), the following equation can be obtained from the (7), (8) and (35):

$$\dot{\omega}_m = \frac{1}{J_m} 1.5 p_n \psi_f \left(i_q' - B_a \omega_m \right) - \frac{B_m}{J_m} \omega_m \quad (36)$$

The poles of the (36) are assigned to the desired closed-loop bandwidth α, and the transfer function of the rotational speed relative to the q-axis current can be obtained as follows.

$$\omega_m(s) = \frac{1.5 p_n \psi_f / J_m}{s + \gamma} i_q'(s) \quad (37)$$

The coefficient B_a of active damping can be obtained by comparing the (36) and (37), and shown as follows.

$$B_a = \frac{\gamma J_m - B_m}{1.5 p_n \psi_f} \quad (38)$$

If the traditional PI controller is used, the expression of the speed loop controller is shown as follows [33].

$$\begin{cases} i_d^* = 0 \\ i_q^* = \left(k_p + \frac{k_i}{s} \right) (\omega_r - \omega_m) - B_a \omega_m \end{cases} \quad (39)$$

Therefore, the parameters k_p and k_i of PI controller can be set by the following formula [34].

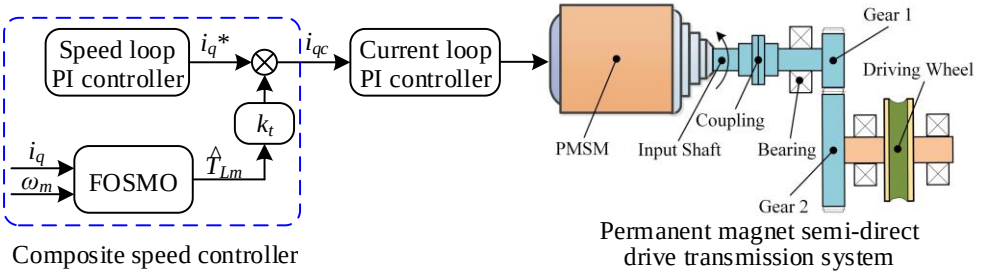

FIGURE 6. Schematic diagram of anti-disturbance speed control strategy for permanent magnet semi-direct drive transmission system.

$$\begin{cases} k_p = \dfrac{\gamma J_m}{1.5 p_n \psi_f} \\ k_i = \gamma k_p \end{cases} \tag{40}$$

where α is the desired frequency bandwidth of the speed loop. Compared with the typical II system, the parameter tuning method in this paper is simpler, and the relationship between the parameter adjustment and the dynamic quality of the speed is clearer.

B. DESIGN OF COMPOSITE SPEED CONTROLLER

Finally, the observed value of the designed FOSMO is used as the compensation control input of the speed controller, and the load disturbance of PMSM is compensated in real time. The schematic diagram is shown in Fig. 6. It is assumed that the output of the PI speed controller is i_{qc}, the observed value of the designed FOSMO is $\hat{T}_{Lm}$, the compensation gain of load disturbance is k_t, and the output of the anti-disturbance composite speed controller (PI+FOSMO) is shown as follows.

$$i_{qc} = i_q^* + k_t \hat{T}_{Lm} \tag{41}$$

C. ANTI-SATURATION DESIGN OF COMPOSITE SPEED CONTROLLER

In the actual operation of the permanent magnet semi-direct drive transmission system of the overhead manned equipment, there are various physical limitations in the control system, such as the variation range limitation of the motor current and speed. It causes the inconsistency between the actual control input and output, leading to the saturation phenomenon of the control system, and weakening the performance of the speed controller.

Similarly, the control output i_{qc} of the composite speed controller cannot be arbitrarily large. That is to say, the control output of the composite speed controller has upper and lower limits, and can be assumed as $i_{qc\max}$ and $i_{qc\min}$ respectively. In order to protect the control system, a saturation limit must be added to the control output of the composite speed controller, which can be expressed as follows.

$$i_{qo} = \begin{cases} i_{qc\max}, & i_{qc} \geq i_{qc\max} \\ i_{qc}, & i_{qc\min} < i_{qc} < i_{qc\max} \\ i_{qc\min}, & i_{qc} \leq i_{qc\min} \end{cases} \tag{42}$$

When the saturation limit is added to the (42), the actual control input of the current loop will be inconsistent with the control output of the composite speed controller. At this time, the sudden change of load torque in a wide range may cause greater speed control fluctuations, and even cause system instability in severe cases [35]. Therefore, in order to improve the dynamic performance of the PMSM control system, it is necessary to add an anti-saturation link in the composite speed controller to reduce the influence of the saturation phenomenon.

The main goal of the anti-saturation design of the composite speed controller is to make the system's saturated output performance close to the linear output without saturation [36]. Scholars at home and abroad have proposed many anti-saturation methods, such as the conditional integration method, inverse calculation tracking method, anti-reset windup method, etc. Among them, the anti-reset windup method is a linear feedback using the restricted loop. For the designed composite speed controller, the improved anti-reset windup method is used to realize the anti-saturation design of the composite speed controller, and as shown in Fig. 7.

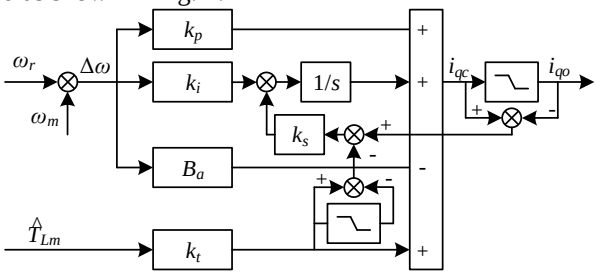

FIGURE 7. Anti-saturation principle of composite speed controller.

V. RESULTS AND ANALYSIS

The load torque of the overhead manned equipment is applied to the semi-direct drive transmission system output shaft through the driving wheel. Assume that the load torque of the overhead manned equipment has a constant load (800N.m) from 0 to 2s, and there is a sudden load and random load with sinusoidal shape at t = 2s, as shown in Fig. 8a. The load torques T_{Lm} applied to the PMSM output shaft are shown in Fig. 8b. Among them, the curve of T_{Lms} does not consider the nonlinear gear meshing characteristics in the semi-direct drive transmission system. The curve of T_{Lmc} considers the nonlinear gear meshing characteristics

which are obtained according to the established dynamic model of the semi-direct drive transmission system, and it is closer to the actual load characteristics of system. Comparing the two curves in the Fig. 8b, it can be seen that in the actual permanent magnet semi-direct drive transmission system, the nonlinear gear meshing transmission leads to the complex load characteristics on the PMSM output shaft. This complex load characteristic will seriously affect the stability of the speed control system of the PMSM, and then challenge the safety of the permanent magnet semi-direct drive transmission system of overhead manned equipment.

The parameters of the PMSM are shown in Table I. The parameters of the semi-direct drive transmission system are shown in Table II.

According to the vector control principle of PMSM, the simulation model of the anti-disturbance speed control strategy of the permanent magnet semi-direct drive transmission system can be established based on MATLAB/Simulink, and as shown in Fig. 9.

TABLE I
SIMULATION PARAMETERS OF PMSM.

	Rated power (kW)	Rated speed (r/min)	Rated torque (N.m)	Stator resistance (Ω)	Flux linkage (Wb)	*d*-axis inductance (mH)	*q*-axis inductance (mH)	Pole pairs number	Rotational inertia (kg.m^2)
PMSM	37	300	1209	0.116	1.235	4.28	4.28	8	1.96

TABLE II
SIMULATION PARAMETERS OF THE SEMI-DIRECT DRIVE TRANSMISSION SYSTEM.

	Teeth number	Modulus (mm)	Teeth width (mm)	Pressure angle (°)	Aperture (mm)
Gear 1	17	6	100	20	80
Gear 2	105	6	100	20	180

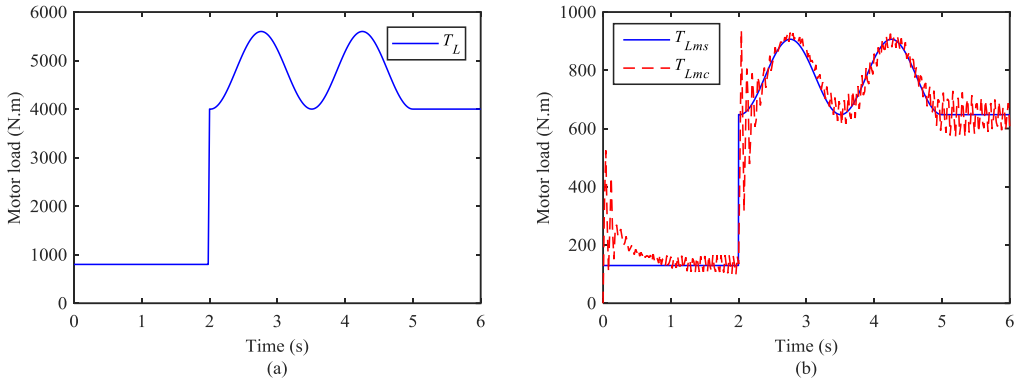

FIGURE 8. Simulated load of permanent magnet semi-direct drive transmission system: (a) simulated load torque of driving wheel of semi-direct drive transmission system; (b) load torque of PMSM output shaft.

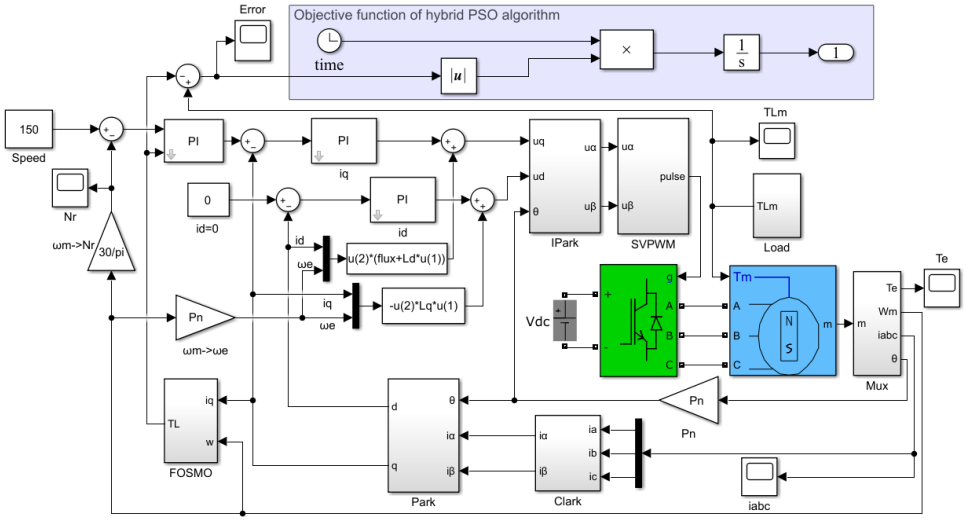

FIGURE 9. Simulation model of anti-disturbance speed control strategy for permanent magnet semi-direct drive transmission system.

A. PI SPEED CONTROLLER

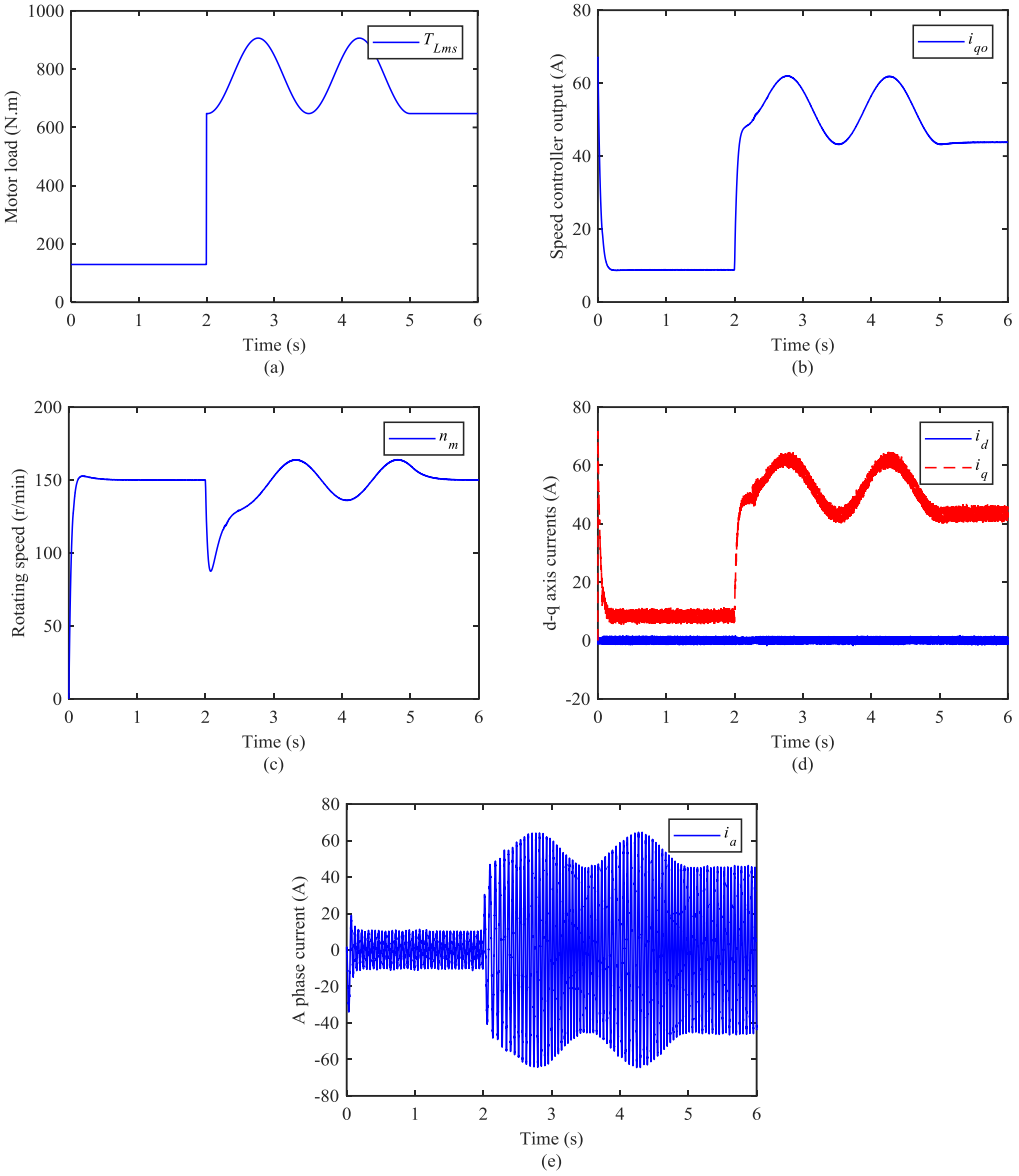

FIGURE 10. Result curves of PI speed controller without considering the nonlinear gear meshing characteristics: (a) load torque; (b) control output of PI speed controller; (c) rotating speed; (d) d-q axis currents; (e) A phase current.

When the nonlinear gear meshing characteristics of the semi-direct drive transmission system are not considered, the control effect of the PI speed controller is shown in Fig. 10. Fig. 10a shows the load torque curve of the PMSM. Fig. 10b shows the control output curve of the PI speed controller. It can be seen that the PI speed controller does not reach the output saturation (limiting [-80, 80]), and the control output of the PI speed controller is close to the load torque curve. Fig. 10c shows the rotating speed curve of PMSM. There is a certain overshoot in the starting process, and the PI controller can ensure the stability of speed control under constant load. When the load changes suddenly (at t=2s), there is a significant decrease in the speed curve, and the speed curve will fluctuate under the subsequent load fluctuation conditions. Fig. 10d shows the *d-q* axis current curves of the PMSM. Fig. 10e shows the A phase current curves of the PMSM.

When the nonlinear gear meshing characteristics of the semi-direct drive transmission system are considered, the control effect of the PI speed controller is shown in Fig. 11. Fig. 11a shows the load torque curve of the PMSM. Fig. 11b shows the control output curve of the PI speed controller. It can be seen that the PI speed controller does not reach the output saturation (limiting [-80, 80]). Fig. 11c shows the rotating speed curve of PMSM. Compared to the Fig. 10c, the complex load characteristic (as shown in Fig. 11a) causes the speed control to fluctuate all the time, which cannot be guaranteed in a stable state. At this time,

not only the smooth and stable operation of the overhead manned equipment cannot be guaranteed, but the safety of the system may even be endangered. Fig. 11d shows the *d-q* axis current curves of the PMSM. Fig. 11e shows the A phase current curves of the PMSM.

According to the above analysis of Fig. 10 and Fig. 11, under the condition of constant load, the designed PI controller can meet the stable speed control requirements of the PMSM. But the disturbances such as load mutation and fluctuation seriously affect the stability of the speed control, and then challenge the safety of the permanent magnet semi-direct drive transmission system of overhead manned equipment. Therefore, it is necessary to identify the load disturbance and compensate it to the speed control system to improve the stability of the control system. In addition, compared with Fig. 10a, the load characteristic shown in Fig. 11a are more complex and closer to the actual load characteristics of the permanent magnet semi-direct drive transmission system. So, the following study only uses the load characteristics shown in Fig. 11a to verify the effectiveness.

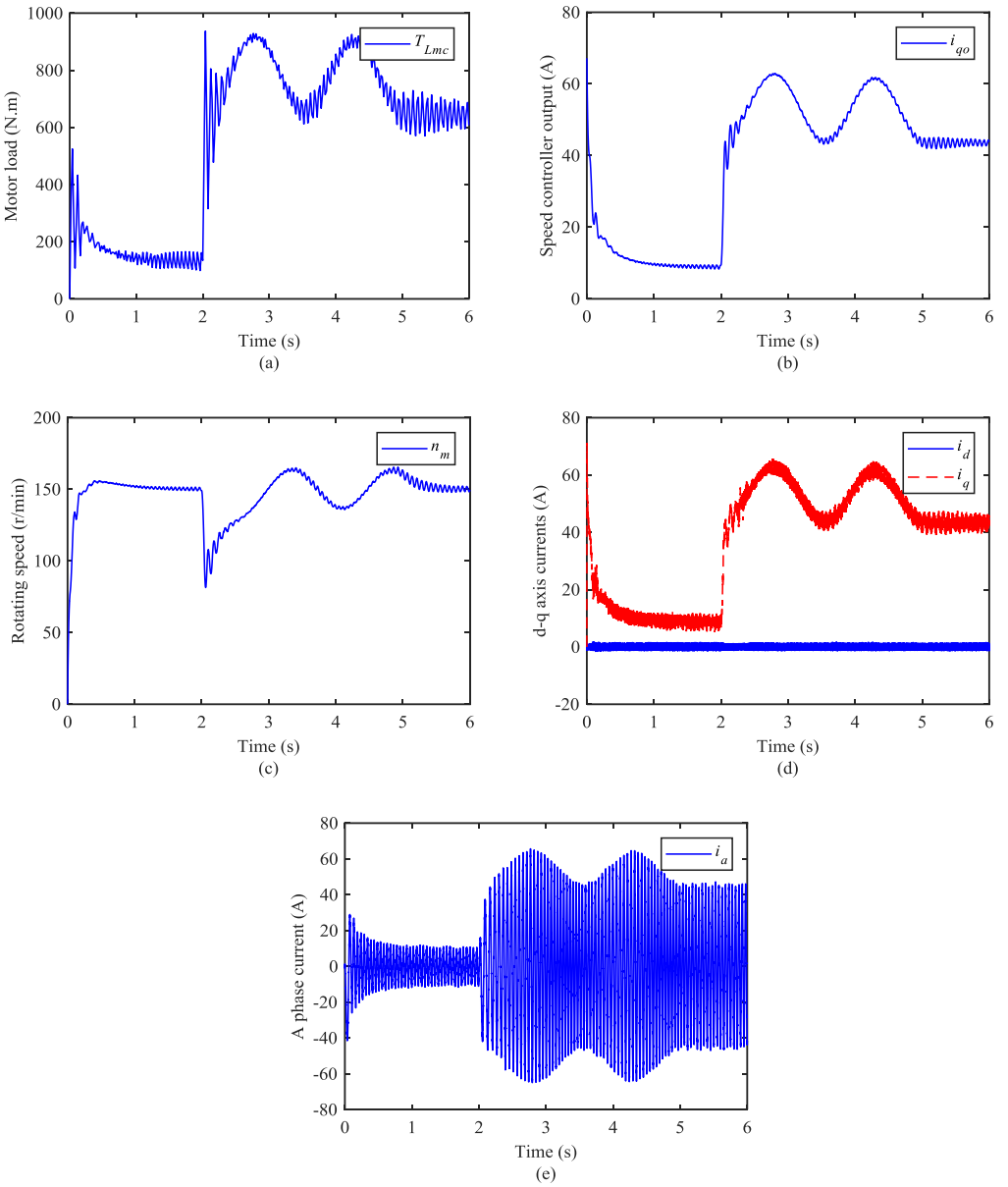

FIGURE 11. Result curves of PI speed controller considering nonlinear gear meshing characteristics: (a) load torque; (b) control output of PI speed controller; (c) rotating speed; (d) d-q axis currents; (e) A phase current.

This article has been accepted for publication in IEEE Access. This is the author's version which has not been fully edited and content may change prior to final publication. Citation information: DOI 10.1109/ACCESS.2022.3214205

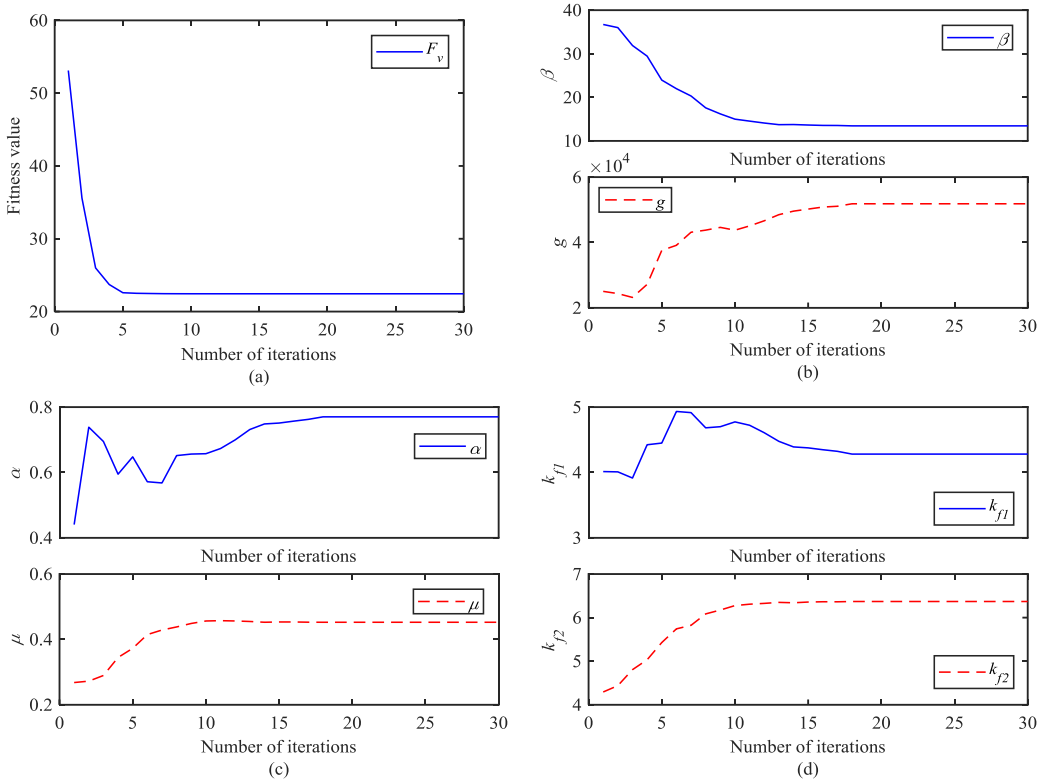

FIGURE 12. **Parameter optimization results of FOSMO based on the hybrid PSO algorithm: (a) convergence chart of fitness value; (b) optimization curves of parameter β and g; (c) optimization curves of parameter α and μ; (d) optimization curves of parameter k_{f1} and k_{f2}.**

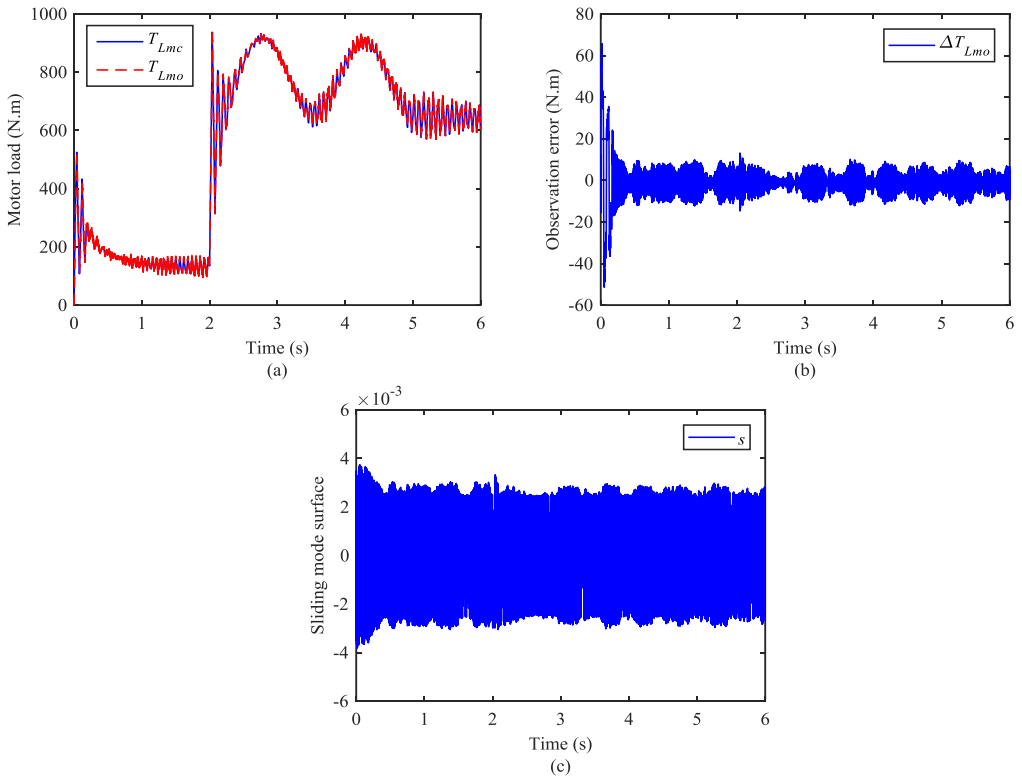

FIGURE 13. **Load disturbance observation curves of the traditional SMO: (a) load torque and observation values; (b) observation error; (c) sliding mode surface.**

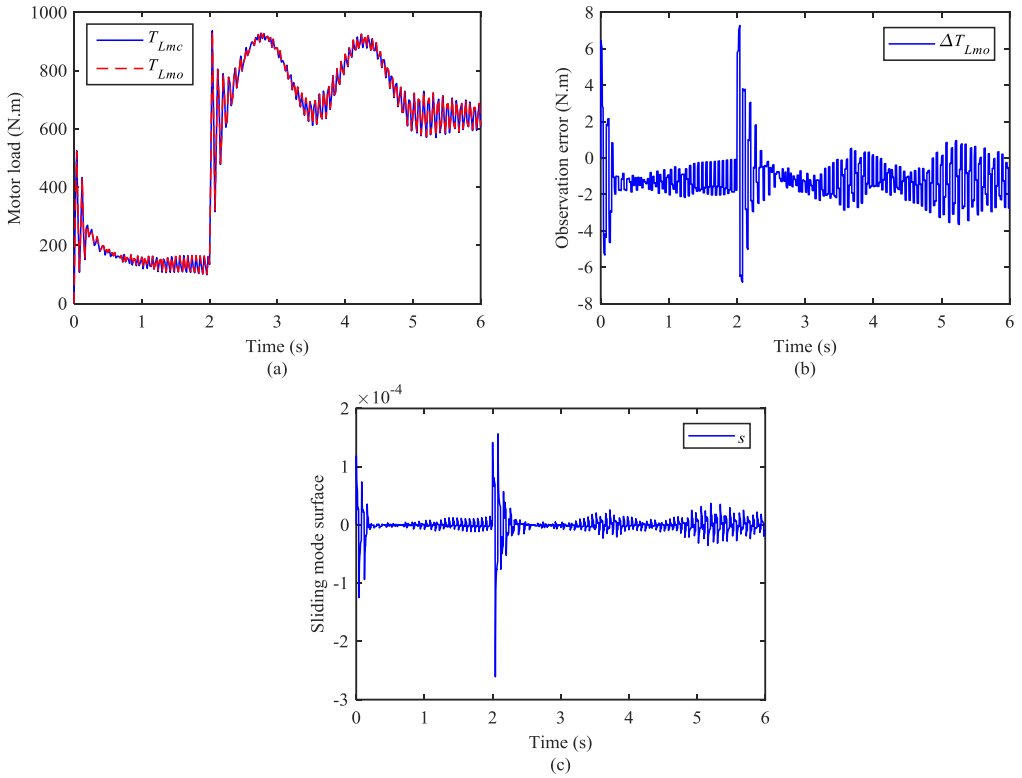

FIGURE 14. Load disturbance observation curves of the designed FOSMO: (a) load torque and observation values; (b) observation error; (c) sliding mode surface.

B. LOAD DISTURBANCE OBSERVER

The designed FOSMO contains parameters α, β, g, μ, p, q, k_{f1}, k_{f2}, etc. Among them, p and q are positive odd numbers, and $1<p/q<2$. Therefore, the p and q parameters are easy to be selected by manual methods, and p and q are chosen as 9 and 7 respectively. This paper uses the hybrid PSO algorithm designed in Section 3.3 to optimize the remaining parameters (α, β, g, μ, k_{f1}, k_{f2}), and the optimization ranges of α, β, g, μ, k_{f1}, k_{f2} are selected as [0, 1], [1e-5, 100], [10000, 80000], [0, 1], [0, 10], [0, 10], respectively. The fitness value and parameter change curves of the hybrid PSO algorithm are shown in Fig. 12. According to the optimization results of the hybrid PSO algorithm, the parameters of FOSMO are α=0.7702, β=13.46, g=51800, μ=0.4525, k_{f1}=6.37, k_{f2}=4.281, respectively.

To illustrate the effectiveness of the FOSMO designed in this paper, it is compared with the traditional SMO in the literature [15-17], and the load disturbance observation results of the traditional SMO and the designed FOSMO are shown in Fig. 13 and Fig. 14 respectively. From the comparison curves of the load torque and observed results shown in Fig. 13a and Fig. 14a, it can be seen that both SMO and FOSMO can realize the load disturbance observation on the PMSM output shaft. Furthermore, the load observation curve of FOSMO is smoother and the buffeting is smaller. From the load observation error curves shown in the Fig. 13b and Fig. 14b, compared with the traditional SMO, the observation error of the designed FOSMO is smaller. From the sliding mode surface curves shown in the Fig. 13c and Fig. 14c, compared with the traditional SMO, there is almost no chattering on the sliding surface of the designed FOSMO. It proves that the method proposed in this paper can effectively suppress the chattering of the sliding mode surface and improve the load observation accuracy at the same time.

C. COMPOSITE SPEED CONTROLLER

Through the above analysis, the FOSMO with better performance is selected to observe the load disturbance of the PMSM system. According to the principle shown in Fig. 6, the observed value of load disturbance is used as the compensation control input of the speed controller, and the results are shown in Fig. 15. Fig. 15a shows the comparison curves between the load torque and the observation values, which proves that the FOSMO realizes the load disturbance observation on the PMSM output shaft. Fig. 15b shows the load observation error. Fig. 15c shows the sliding mode surface. Fig. 15d shows the control output of the composite speed controller (PI+FOSMO), and it also does not reach the output saturation (limiting [-80, 80]). From the speed curve shown in Fig. 15e, it can be seen that the designed composite speed controller (PI+FOSMO) can realize the stable speed control of the PMSM under complex load disturbance conditions. Therefore, the load disturbance compensation method is effective and can ensure the dynamic performance and operational safety of the

permanent magnet semi-direct drive transmission system of the overhead manned equipment. Fig. 15f shows the *d-q* axis current curves of the PMSM. Fig. 15g shows the A phase current curve of the PMSM.

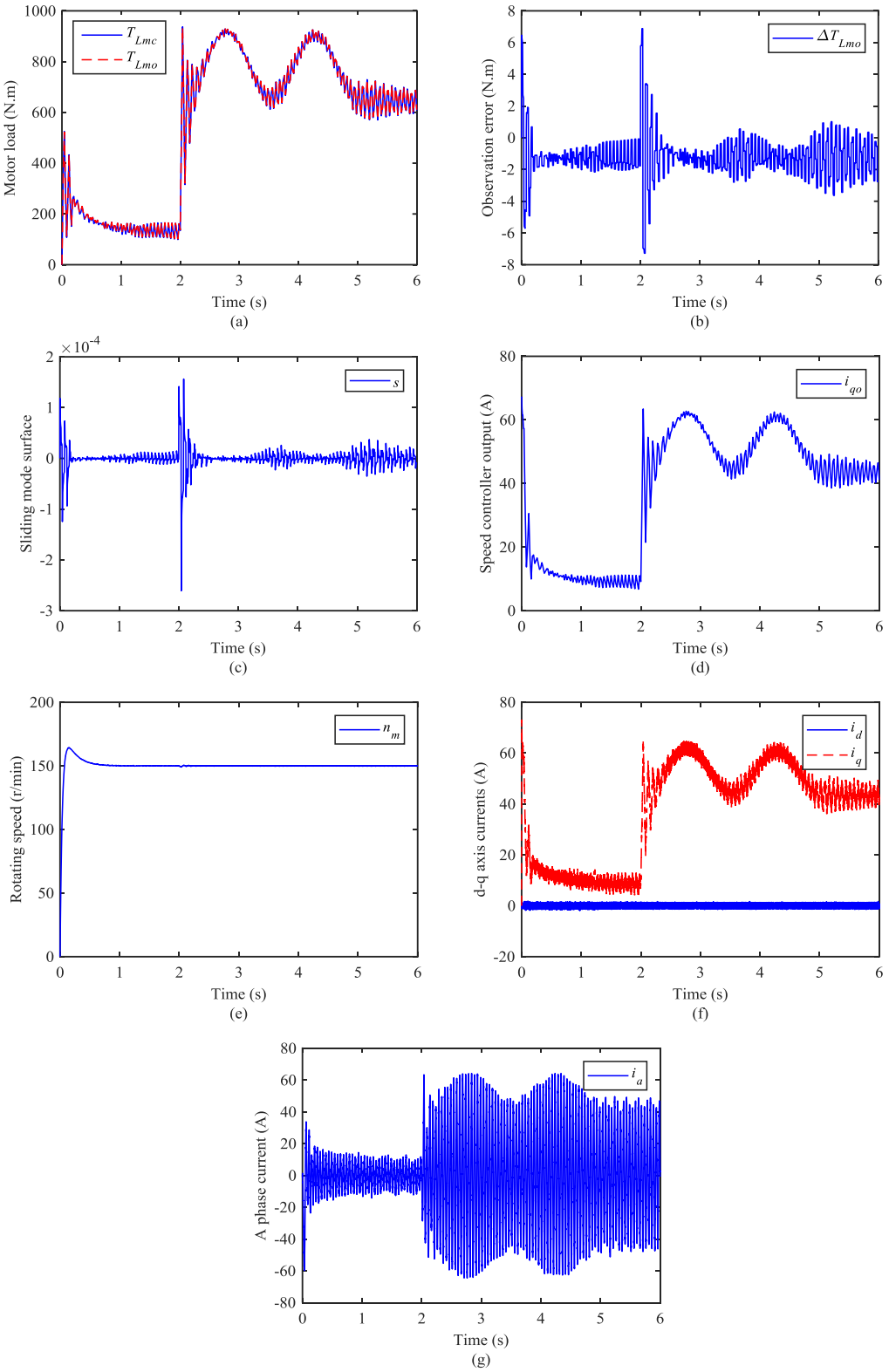

FIGURE 15. Result curves of anti-disturbance composite speed controller: (a) load and observation values; (b) observation error; (c) sliding mode surface; (d) control output of composite speed controller; (e) rotating speed; (f) d-q axis currents; (g) A phase current.

D. ANTI-SATURATION OF COMPOSITE SPEED CONTROLLER

In order to verify the effect of the designed anti-saturation composite speed controller under control saturation, the load torque of PMSM shown in Fig. 11a is increased by 33%, and the comparison curves between the composite speed controller and the anti-saturation composite speed controller are shown in Fig. 16. Fig. 16a shows the comparison curves between the load torque and the observation values, which proves that the accurate load observation can still be achieved under the control saturation condition. Fig. 16b shows the load observation error. Fig. 16c shows the sliding mode surface. Fig. 16d shows the control output of the composite speed controller and anti-saturation composite speed controller. It can be seen that the output of the composite speed controller is limited to -80-80 due to the effect of control output limiting. From the speed curves shown in Fig. 16e, it can be seen that the composite speed controller will not have speed overshoot when the control output is saturated. The added anti-saturation link improves the performance of the composite speed controller and achieves the expected purpose. Fig. 16f shows the *d-q* axis current curves of the PMSM. Fig. 16g shows the A phase current curve of the PMSM.

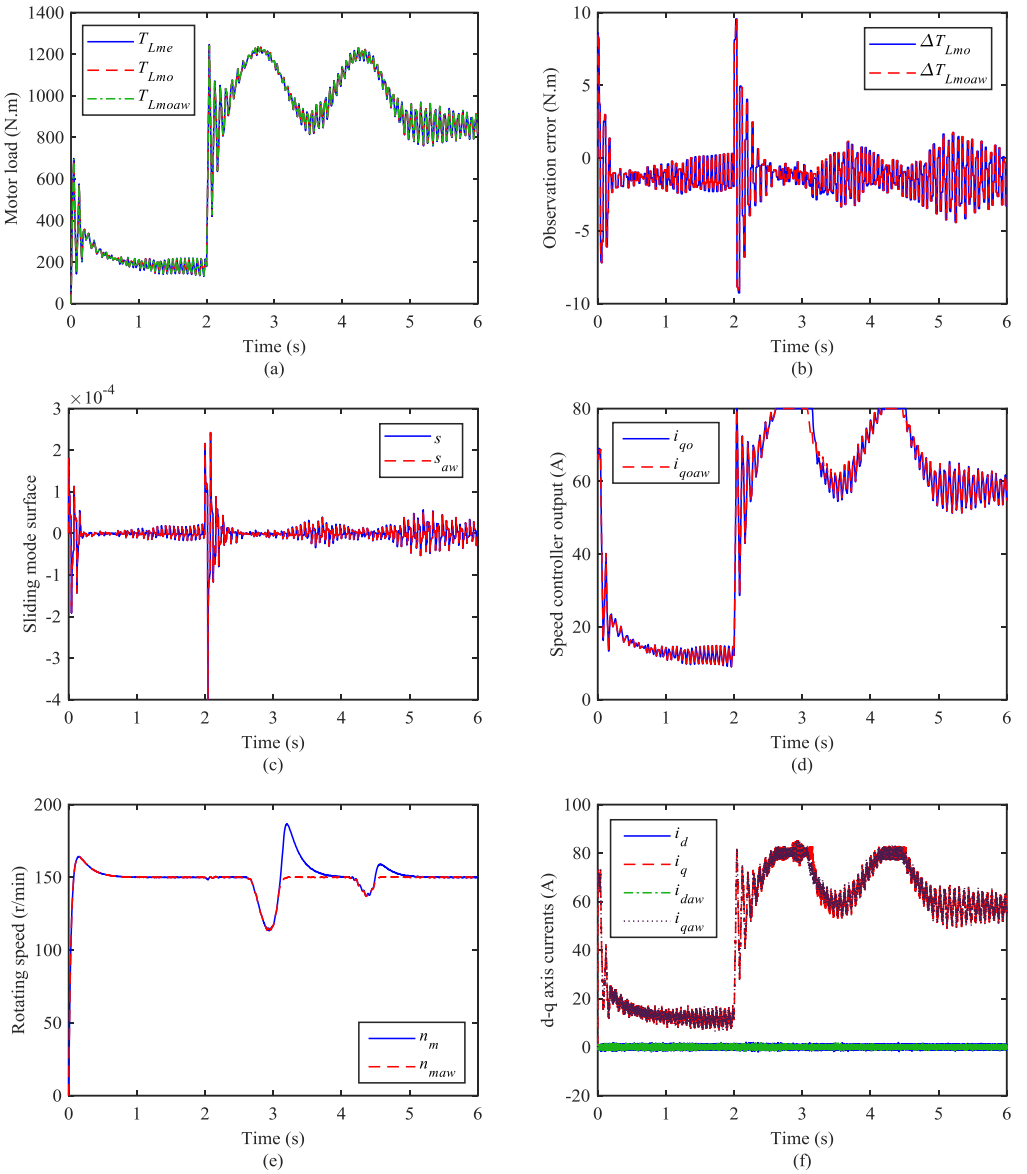

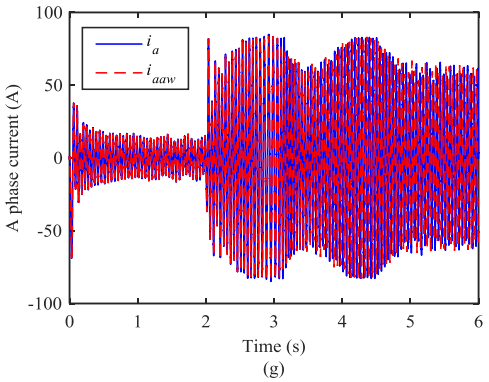

FIGURE 16. Comparison curves of composite speed controller and anti-saturation composite speed controller under control saturation: (a) load and observation values; (b) observation error; (c) sliding mode surface; (d) control output of composite speed controller; (e) rotating speed; (f) d-q axis currents; (g) A phase current.

VI. CONCLUSIONS

In this paper, an anti-disturbance composite speed control method based on the PI speed controller and FOSMO is proposed for the permanent magnet semi-direct drive transmission system of overhead manned equipment. The designed FOSMO combines the advantages of nonsingular terminal sliding mode and fractional order theory, reducing the chattering of the sliding mode surface, which accurately observing the load disturbance of the permanent magnet semi-direct drive transmission system. Subsequently, the speed loop PI controller is designed with the concept of "active damping", and the FOSMO is combined to build the composite speed controller (PI+FOSMO). Furthermore, the designed composite speed controller is further improved by anti-saturation design and parameter optimization. Finally, the effectiveness of the proposed method is verified based on the load characteristics of the permanent magnet semi-direct drive transmission system of the overhead manned equipment.

Under the load characteristics of the permanent magnet semi-direct drive transmission system of the overhead manned equipment, the designed PI speed controller can ensure the safe operation of the PMSM, but there is a large speed control fluctuation in the case of load fluctuations. Then, the hybrid PSO algorithm is used to optimize the parameters of the designed FOSMO. Comparing the results of FOSMO and traditional SMO, it can be seen that the designed FOSMO can realize the observation of complex load disturbances, and the observation error is smaller. The sliding mode surface of FOSMO is smoother and there is almost no chattering. Therefore, the designed FOSMO has better performance, which can effectively suppress chattering and ensure the accuracy of load observation. Subsequently, the designed composite speed controller (PI+FOSMO) realizes the speed stability control of the permanent magnet semi-direct drive transmission system under complex load disturbance, which proves that the scheme of compensating the observed value of load disturbance into the speed controller is effective, and makes up for the shortcomings of speed control fluctuation caused by load disturbance. After that, the comparison results under the control output saturation condition show that the improved composite speed controller with anti-saturation link has less speed fluctuation and better performance. Therefore, the method proposed in this paper realizes the anti-disturbance ability of the permanent magnet semi-direct drive transmission system, and improves the dynamic performance while ensuring the stability of the control system.

ACKNOWLEDGMENT

This work was supported by the National Natural Science Foundation of China (No. 52005220 and No. 51775543), China Postdoctoral Science Foundation Grant (2019M651962) and A Project Funded by the Priority Academic Program Development of Jiangsu Higher Education Institutions (No. PAPD-2018-87).

REFERENCES

[1] Zhang XG, Zhao ZK, Liu JG, et al. "A novel mechanical design of broken rope protection device for enhancing the safety performances of overhead manned equipment in coal mine". *Advances in Mechanical Engineering*, vol. 7, no. 8, pp. 1-10, 2015.

[2] Sheng LC, Li W, Wang YQ, et al. "Nonlinear dynamic analysis and chaos control of multi-freedom semi-direct gear drive system in coal cutters". *Mechanical Systems and Signal Processing*, vol. 116, pp. 62-77, 2019.

[3] Petrovic V, Ortega R, Stankovic AM, et al. "Design and implementation of an adaptive controller for torque ripple minimization in PM synchronous motors". *IEEE Transactions on Power Electronics*, vol. 15, pp. 871-880, 2000.

[4] Li SH and Gu H. "Fuzzy adaptive internal model control schemes for PMSM speed-regulation system". *IEEE Transactions on Industrial Informatics*, vol. 8, no. 4, pp. 767-779, 2012.

[5] Yu JP, Shi P, Dong WJ, et al. "Neural network-based adaptive dynamic surface control for permanent magnet synchronous motors". *IEEE Transactions on Neural Networks & Learning Systems*, vol. 26, no. 3, pp. 640-645, 2015.

[6] Sadala SP, Patre BM. "A new continuous sliding mode control approach with actuator saturation for control of 2-DOF helicopter system". *ISA Transactions*, vol. 74, pp. 165-174, 2018.

[7] Wu Fei, Li Penghan, and Wang Jie. "FO improved fast terminal sliding mode control method for permanent-magnet synchronous motor with FO disturbance observer". *IET Control Theory & Applications*, vol. 13, no. 10, pp. 1425-1434, 2019.

[8] Lu E, Li W, Wang SB, et al. "Disturbance rejection control for PMSM using integral sliding mode based composite nonlinear feedback control with load observer". *ISA transactions*, vol. 116, pp. 203-217, 2021.

[9] Xu Yongxiang, Li Shaobin, Zou Jibin. "Integral sliding mode control based deadbeat predictive current control for PMSM crives with disturbance rejection". *IEEE Transactions on Power Electronics*, vol. 37, no. 3, pp. 2845-2856, 2022.

[10] Tety P, Konate A, Asseu O, et al. "A robust extended Kalman filter for speed-sensorless control of a linearized and decoupled PMSM drive". *Engineering*, vol. 7, pp. 691-699, 2015.

[11] Yu JP, Shi P, Dong Wj, et al. "Neural network-based adaptive dynamic surface control for permanent magnet synchronous motors". *IEEE Transactions on Neural Networks & Learning Systems*, vol. 26, no. 3, pp. 640-645, 2015.

[12] Zhou Z, Zhang B, Mao D. "Robust sliding mode control of PMSM based on a rapid nonlinear tracking differentiator and disturbance observer". *Sensors*, vol. 18, no. 1031, pp. 1-9, 2018.

[13] Hou QK and Ding SH. "Finite-time extended state observer-based super-twisting sliding mode controller for PMSM drives with inertia identification". *IEEE Transactions on Transportation Electrification*, vol. 8, no. 2, pp. 1918-1929, 2022.

[14] Sun XD, Zhang Y, Lei G, et al. "An improved deadbeat predictive stator flux control with reduced-order disturbance observer for in-wheel PMSMs". *IEEE/ASME Transactions on Mechatronics*, vol. 27, no. 2, pp. 690-700, 2022.

[15] Lu E, Li W, Yang XF, et al. "Composite sliding mode control of a permanent magnet direct-driven system for a mining scraper conveyor". *IEEE Access*, vol. 5, pp. 22399-22408, 2017.

[16] Xu B, Zhang L, Ji W. "Improved non-singular fast terminal sliding mode control with disturbance observer for PMSM drives". *IEEE Transactions on Transportation Electrification*, vol. 7, no. 4, pp. 2753-2762, 2021.

[17] Zhang XG, Li ZX. "Sliding-mode observer-based mechanical parameter estimation for permanent magnet synchronous motor". *IEEE Transactions on Power Electronics*, vol. 31, no. 8, pp. 5732-5745, 2016.

[18] Lu E, Li W, Yang XF, et al. "Anti-disturbance speed control of low-speed high-torque PMSM based on second-order non-singular terminal sliding mode load observer". *ISA transactions*, vol. 88, pp. 142-152, 2019.

[19] Ke DL, Wang FX, He L, et al. "Predictive current control for PMSM systems using extended sliding mode observer with Hurwitz-based power reaching law". *IEEE Transactions on Power Electronics*, vol. 36, no. 6, pp. 7223-7232, 2021.

[20] Jiang S, Li W, Wang YQ, et al. "Study on electromechanical coupling torsional resonance characteristics of gear system driven by PMSM: a case on shearer semi-direct drive cutting transmission system". *Nonlinear Dynamics*, vol. 104, no. 2, pp. 1205-1225, 2021.

[21] Qin Datong, Xie Liyang. "Modern handbook of mechanical design". 2nd Edition, China: Chemical Industry Press, 2019.

[22] Samko SG, Kilbas AA, Marichev OI. "Fractional integrals and derivatives-theory and applications". Gordon and Breach Science Publishers, New York, 1993.

[23] Li P. "Research and application of traditional and higher-order sliding mode control". National University of Defense Technology, 2011.

[24] Yang GY, Chen SY. "Piecewise fast multi-power reaching law: Basis for sliding mode control algorithm". *Measurement and Control*, vol. 53, no. 9-10, pp. 1929-1942, 2020.

[25] Liu JX. "Research on IPMSM sensorless rotor position estimation". Harbin Institute of Technology, 2010.

[26] Khalil HK. "Nonlinear systems". 3rd Edition, Upper Saddle River, New Jersey: Prentice-Hall, 2002.

[27] Khanh PQ, Anh HPH. "Novel sensorless PMSM speed control using advanced fuzzy MRAS algorithm". *Arabian Journal for Science and Engineering*, vol. 4, pp. 1-12, 2022.

[28] Kennedy J, Eberhart R. "Particle swarm optimization". *IEEE International Conference on Neural Networks*, Perth, Australia, 1995, pp. 1942-1948.

[29] Essam HH, Ahmed GG, Kashif Hussain, et al. "Major advances in particle swarm optimization: theory, analysis, and application". *Swarm and Evolutionary Computation*, vol. 63, pp. 1-39, 2021.

[30] Lim WH, MatIsa NA. "Adaptive division of labor particle swarm optimization". *Expert Systems with Applications*, vol. 42, no. 14, pp. 5887-5903, 2015.

[31] Cai LW and Li X. "Improvement on crossover operation of genetic algorithms". *Systems Engineering and Electronics*, vol. 28, no. 6, pp. 925-928, 2006.

[32] Harnefors F, Pietilainen K, Gertmar L. "Torque-maximizing field-weakening control: design, analysis and parameter selection". *IEEE Transaction on Industrial Electronics*, vol. 48, no. 1, pp. 161-168, 2001.

[33] Chan TF, Wang W, Borsje P, et al. "Sensorless permanent-magnet synchronous motor drive using a reduced-order rotor flux observer". *IET Electric Power Applications*, vol. 2, no. 2, pp. 88-98, 2008.

[34] Yuan L, Shen JQ, Xiao F, et al. "Nonsingular terminal sliding-mode observer design for interior permanant magnet synchronous motor drive at very low-speed". *Acta Physica Sinica*, vol. 62, no. 3, pp. 45-53, 2013.

[35] Chu YZ, Guo QQ, Qi SM, et al. "Study of novel sliding mode control with anti-windup for permanent magnet synchronous motor". *Electric Machines and Control Application*, vol. 43, no. 9, pp. 38-43, 2016.

[36] Mo LL, Liu YQ, Zhang Y. "A study on anti-saturation SMC of SPMSM based on anti-reset windup". *2019 IEEE 3rd Information Technology, Networking, Electronic and Automation Control Conference (ITNEC 2019)*, Guangdong, China, 2019, pp. 1931-1935.

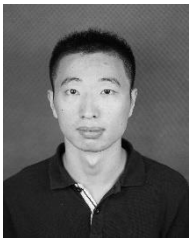

En Lu was born in 1990. He received his bachelor's and doctoral degrees from School of Mechatronic Engineering, China University of Mining and Technology, Xuzhou, China in 2013 and 2018, respectively. From 2018 to 2021, he worked as an assistant researcher at the School of Agricultural Engineering, Jiangsu University, where he was an associate researcher in 2021. His research interests include dynamic analysis, control of PMSM, automatic navigation and path planning.

Wei Li was born in 1964 the B.E. He received degree from the School of Automation Engineer, University of Electronic Science and Technology of China, Chengdu, China, in 1986, and the M.E. and Ph.D. degrees from the China University of Mining and Technology, Xuzhou, China, in 1989 and 2004, respectively. From 1989 to 2004, he shifted and promoted to a Lecturer and Associate Professor with the School of Mechatronic Engineering, China University of Mining and Technology, where he was a Professor in 2005. From 2011 to 2016, he was the Dean of the School of Mechatronic Engineering with the China University of Mining and Technology. His research interests include motor control, mobile target collaboration positioning, metro stray current monitoring, optical fiber sensing and network architecture.

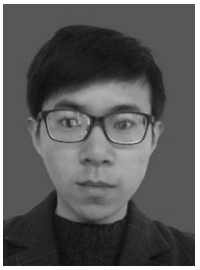

Song Jiang was born in 1995. He received the B.E.and M.E. degree from the School of Mechatronic Engineering, China University of Mining and Technology, Xuzhou, China, in 2017 and 2019, respectively, where he is currently pursuing the Ph.D. degree with the School of Mechatronic Engineering. His research interests include dynamic analysis and control of PMSM.

Yufei Liu was born in 1988. He received his bachelor's and doctoral degrees from China University of Mining and Technology, Xuzhou, China in 2011 and 2016, respectively. Since 2016, he has served as a lecturer and associate professor in the School of Artificial Intelligence, Anhui Polytechnic University. His research interests include electromechanical coupling dynamic analysis and motor control.